ICAS-98-4,4,1

A98-31587

BUCKLING TESTS OF CARBON-EPOXY LAMINATED CYLINDRICAL SHELLS UNDER AXIAL COMPRESSION AND TORSION

Chiara Bisagni
Department of Aerospace Engineering
Politecnico di Milano
Via Golgi 40, 20133 Milano, Italy
e-mail: *chiara@aero.polimi.it*

Abstract

This paper describes an experimental and numerical study, that is part of a research project aiming at improving the knowledge of buckling behaviour of composite shell structures.
The experimental equipment and the methodologies for systematic data acquisition in buckling tests on composite cylindrical shells under axial compression and torsion, applied individually and in combination, are described. Typical results of the first tests performed on carbon-epoxy laminated cylinders are presented, in terms of diagrams, post-buckling patterns and two-dimensional Fourier analysis.
The buckling phenomena is numerically investigated using two finite element codes: ABAQUS and ABAQUS/EXPLICIT. The geometric imperfections measured on the internal surface of the specimens are introduced in the numerical models and the analysis results are compared to the experimental ones. In particular, the numerical analysis is able to follow the evolution of the cylinder shape from the buckling to the post-buckling region.

Introduction

Thin, circular, cylindrical shells are widely used in simple or complex structural configurations, especially in the aerospace industry. On the other side the cylinder is the simplest case of a curved surface. Depending on their use, these shells are subjected to individual and combined application of external loads. In resisting these loads, the structures are subjected to buckling, a physically observed failure mode, which is closely associated with the establishment of its load-carrying capacity.

Therefore, the buckling strength of thin shells along with knowledge of its post-buckling behaviour have been the subject of many researches and investigations both analytical and experimental[1,2,3]. These studies have led to a better understanding of shell behaviour, essential in the safe design of such configuration[4,5,6], but they have considered primarily shells of metallic construction.
More recently, the increasing need for light-weight efficient structures drove structural engineers to the field of structural optimisation and simultaneously to the use of non-conventional materials, such as fibre-reinforced composites, attractive because of their high stiffness - and/or strength - to weight ratios. The studies regarding the buckling phenomena of composite cylindrical shells result much more complicated than in the case of isotropic shells and they have not yet led to systematic and widely applicable design criteria.
In the past few decades, the dominant role of initial imperfections in causing specific shell configurations, particularly circular cylindrical configurations subject to axial compression, to buckle at a load level considerably lower than the value predicted by the classical linearised small deflection theory[7,8] has been recognised and accepted also for composite shells. As a matter of fact, the buckling of composite shells depends also on a large number of input parameters, such as laminae properties and orientations, and can be influenced by several types of imperfections, consequences of the manufacturing process[9], such as thickness variations and local delaminations.
Consequently, a methodology, integrating a reasonable number of experimental tests with a complementary computational activity, appears as the only possible approach[10,11,12,13]. The very large number of input parameters prohibit a pure

21st ICAS Congress
13-18 September 1998
Melbourne, Australia

experimental approach, but, in the meantime, the measurement of relevant properties and response parameters during testing is essential to the development of analytical/numerical procedures and design guidelines for the buckling strength prediction.
The present paper describes the experimental equipment and the methodologies for systematic data acquisition in buckling tests on composite cylindrical shells under axial compression and torsion, applied individually and in combination. Typical results of the first tests performed on carbon fabric cylinders are presented. The test results are compared to numerical analysis performed using two finite element codes: ABAQUS and ABAQUS/EXPLICIT.

Cylindrical shells

The specimens are manufactured and provided by AGUSTA. They are characterised by a length and an internal diameter of 700 *mm*, a thickness of 1.32 *mm* and they present two reinforced tabs at the top and bottom to allow to fix the specimens into the loading rig. The actual length is therefore limited to the central part and is equal to 520 *mm*.
The specimens consist of carbon fabric laid down and the lamina properties are reported in Table 1.
The specimens present two different types of lay-up orientations: [0/45/-45/0] and $[45/-45]_S$. Four nominally identical specimens are available for each lay-up orientation in order to evaluate the repeatability of the buckling tests.

E_{11} E_{22} *[N/mm²]*	52000
G_{12} *[N/mm²]*	2350
ν_{12}	0.302
ρ, density *[kg/mm³]*	1.32×10^{-8}

Table 1 - Lamina properties

Experimental equipment

A loading rig displacement-controlled was designed and constructed to perform buckling tests under axial compression and torsion, applied individually and in combination. The equipment is shown schematically in Figure 1.
To perform axial compression tests, the loading platform is pushed by a hydraulic ram against four ball screw supports placed at the four corners of the platform. At the beginning, the load given by the ram is completely supported by the four screws, which distribute the real applied load on the specimen during the test. In fact, the screws motion is computer-controlled, producing exactly the desired displacement to the loading platform, by means of four stepping motors through four reduction gears. Thus the load level, which is transferred smoothly to the cylinder, depends only on the platform displacement and on the cylinder elastic response and it does not substantially depend on the load magnitude due to the hydraulic ram acting on the platform.
The compression load is measured, during the tests, by means of a load cell situated under the lower clamp, while three LVDT transducers measure the axial displacement of the specimen at three equally spaced points.

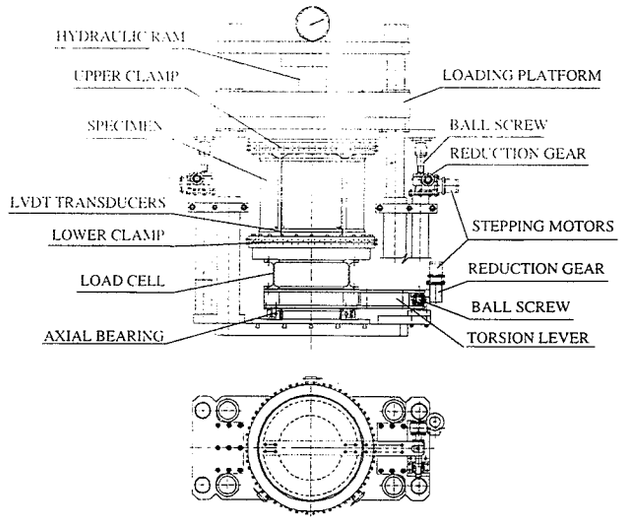

Figure 1 - Experimental equipment

To perform torsion tests, the rotation is given to the specimen bottom by means of a torsion lever. The lever motion is computer-controlled, producing the desired displacement of a screw by means of a stepping motors through a reduction gear, like in the case of axial compression. The load cell, situated under the lower clamp, is able to measure also the torsion, while three LVDT transducers measure the tangential displacement of the specimen bottom at the same three points used during axial compression.
An equipment ad-hoc developed (Figure 2) was designed and constructed to measure the development of the geometric imperfections and of the buckling pattern on the specimen internal surface during the tests[14,15].
The equipment is placed inside the specimen during the tests and consists of a central cylindrical body, connected with a circular plate, fixed in the middle of the specimen lower clamp. The body supports two arms, that hold up a slide, where five laser displacement sensors are placed. The slide can rotate and translate vertically, by means of two stepping motors fixed on the

support. The vertical position of the slide is supplied by an incremental encoder, connected to the worm screw. The starting of every data acquisition is regulated by a photoelectric cell.

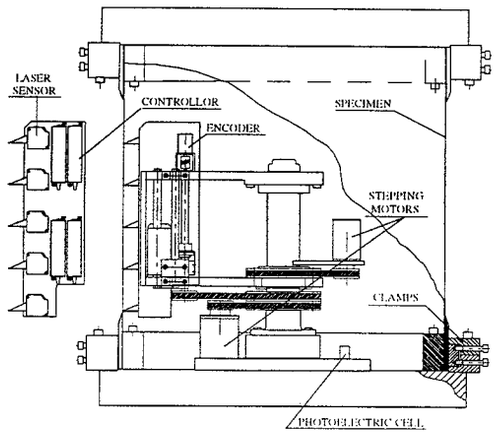

Figure 2 - Equipment to record the specimen internal surface

The five laser displacement sensors are placed at the distance of 40 *mm* from the specimen internal surface. They have a measurement range of ±10 *mm*, with a resolution that depends on the acquisition speed (for acquisition every 2 *ms*, the resolution is 15 μm). So they allow to record both the geometric imperfections, that are some tens of micrometers, and the buckling patterns, which lead to displacements of about 15-20 *mm*. The laser sensors present a great advantage respect to the LVDT transducers previously used to measure the internal surface, because they avoid any contact with the specimens surface and do not influence at all the buckling behaviour.

The all experimental equipment is computer-controlled by means of a software ad-hoc developed in *Visual Basic*, through two multifunction acquisition boards. The measurements of the specimen internal surface are usually recorded in a regular mesh of points 10 *mm* spaced both circumferentially and axially and they refer only to the central part of the cylinder surface, 450 *mm* long. The cylinder's internal surface is recorded immediately before the test and about 15-20 times during the buckling test itself. In fact the time required to measure a complete surface is limited to 4 minutes.

Experimental results

The specimens were axially compressed, recording the compression load vs. the axial displacement and the development of the geometric imperfections, as well as the post-buckling pattern. A specimen for each kind of lay-up orientation was also tested at least two times to check the repeatability.

The values of the measured buckling loads are reported in Tables 2 and 3, where they are compared to the analytical buckling loads, obtained from a classical linear theory, not including the effect of the initial imperfections[15].

The ratio between experimental and analytical buckling load is higher for the $[45/-45]_S$ cylinders than for the [0/45/-45/0] cylinders.

Tables 2 and 3 also report the post-buckling pattern number of waves, in the circumferential and axial direction respectively. Cylinders with the same lay-up orientation develop a post-buckling pattern that is quite always the same. On the other side, cylinders with different lay-up orientation show significant differences on the post-buckling pattern.

Cylinder number	Exp. load *[kN]*	Analyt. load *[kN]*	Exp. / analyt. load	Post-buckl. pattern
1st	172.87	240	0.72	9 x 2
2nd	151.62		0.63	10 x 2
3rd	155.67		0.65	10 x 2
4th	164.70		0.69	10 x 2

Table 2 - Axial compression buckling loads: [0/45/-45/0] cylinders

Cylinder number	Exp. load *[kN]*	Analyt. load *[kN]*	Exp. / analyt. load	Post-buckl. pattern
1st	120.23	120.58	0.99	8 x 1
2nd	116.45		0.97	7 x 1
3rd	102.45		0.85	8 x 1
4th	112.63		0.93	8 x 1

Table 3 - Axial compression buckling loads: $[45/-45]_S$ cylinders

Two typical diagrams of compression load vs. axial displacement are presented in Figures 3 and 4, where both loading and unloading sequences are reported. In the tests on the [0/45/-45/0] cylinders, the buckling load is reached without significant pre-buckling nonlinearities, while pre-buckling non linearities are present during the tests on the $[45/-45]_S$ cylinders. All the tests performed show that buckling phenomena appear suddenly and in any case a load reduction is measured. The tests are continued for a little in post-buckling, leading to further increase of load and displacement. During unloading phase, the diagrams agree with theoretical curves, until the buckling patterns disappear and the values return to coincide with those of the loading sequence.

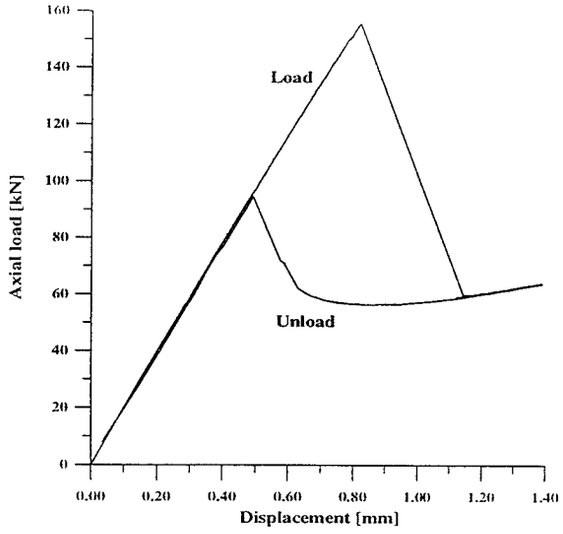

Figure 3 - Diagram of compression load vs. axial displacement: [0/45/-45/0] cylinder

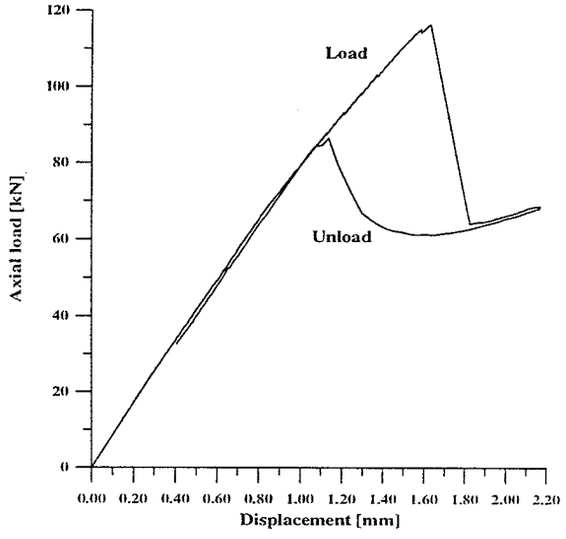

Figure 4 - Diagram of compression load vs. axial displacement: $[45/-45]_S$ cylinder

Figures 5 and 6 report the post-buckling patterns recorded during two tests on carbon fabric cylinders. The patterns are well-defined and perfectly regular. They do not change during the tests, but there is only an increase of the displacements normal to the surface, in the post-buckling region. For the [0/45/-45/0] cylinder, it is possible to point out 9 circumferential waves and 2 axial waves and the displacements normal to the surface reach 11 *mm* internally and 5 *mm* externally in the post-buckling region. The pattern recorded during a test on a $[45/-45]_S$ cylinder shows 8 circumferential waves and 1 axial wave. The displacements normal to the surface reach, in the post-buckling region, 14 *mm* internally and 7 *mm* externally.

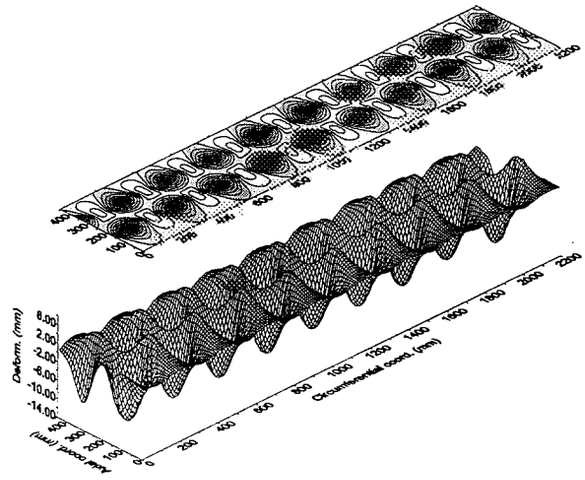

Figure 5 - Post-buckling pattern (9x2) during an axial compression test: [0/45/-45/0] cylinder

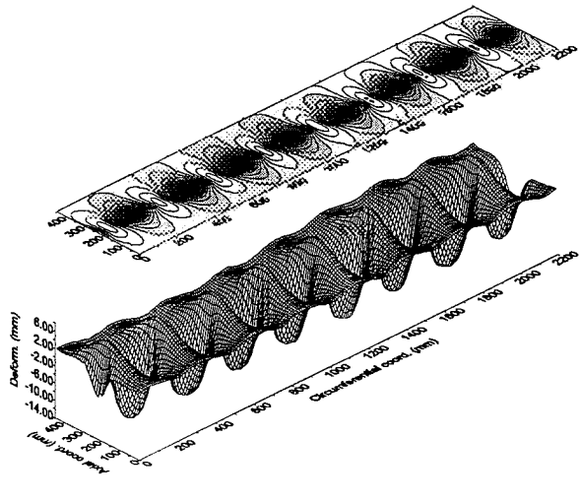

Figure 6 - Post-buckling pattern (8x1) during an axial compression test: $[45/-45]_S$ cylinder

A high-speed film has been realised during a test on a [0/45/-45/0] carbon fabric cylinder, to better understand the dynamics of the buckling phenomena and it was found that the phenomena takes place in about 7/1000 of seconds.

A two-dimensional Fourier analysis[8,9] is performed on all the internal surfaces recorded during each test. Typical plots in terms of double Fourier series coefficients are reported in Figures 7 and 8, where the Fourier coefficients (normalised to the maximum values of the coefficients recorded during each test) are represented in function of the number of the circumferential and axial waves.

Work is currently under way on performing buckling tests under torsion and under axial compression and torsion applied in combination.

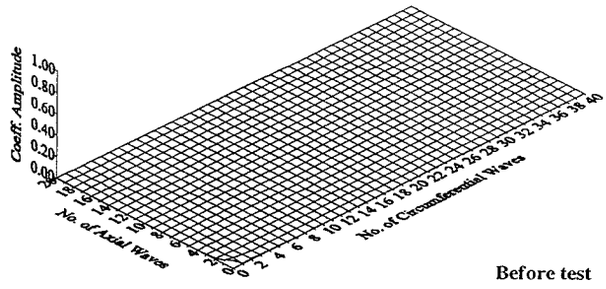

Before test

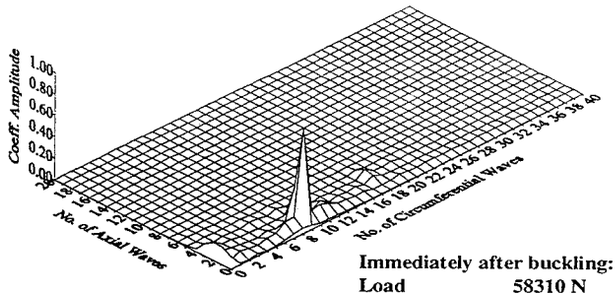

Immediately after buckling:
Load 58310 N
Displacement 1.295 mm

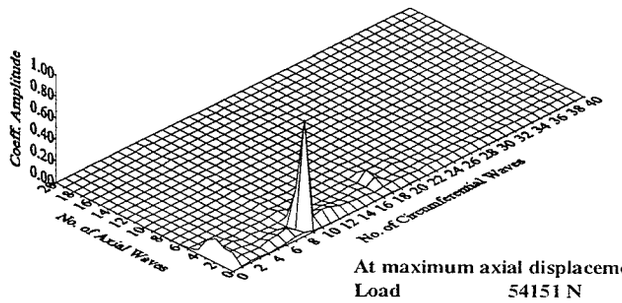

At maximum axial displacement:
Load 54151 N
Displacement 1.460 mm

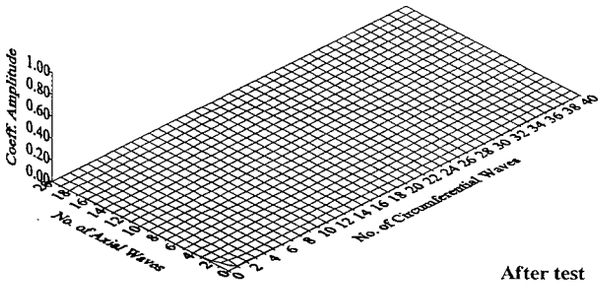

After test

Figure 7 - Two-dimensional Fourier analysis: [0/45/-45/0] cylinder (normalised to 6.54)

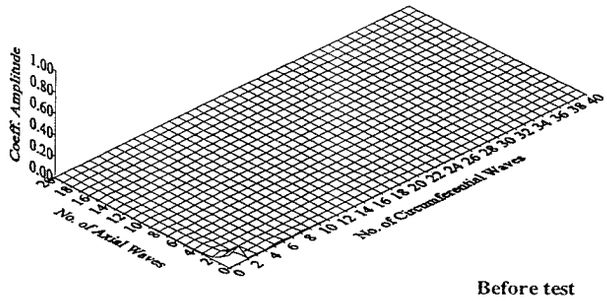

Before test

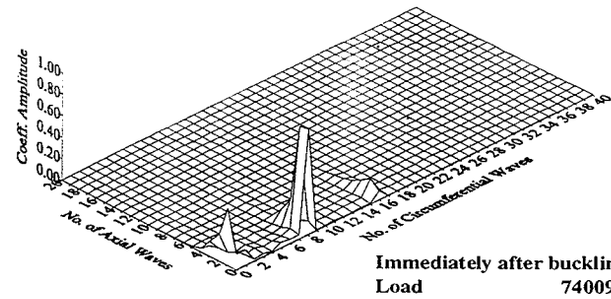

Immediately after buckling:
Load 74009 N
Displacement 1.628 mm

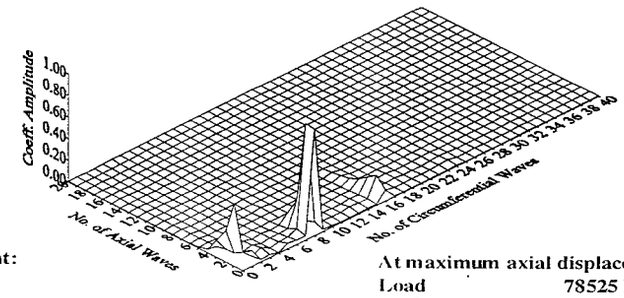

At maximum axial displacement:
Load 78525 N
Displacement 1.848 mm

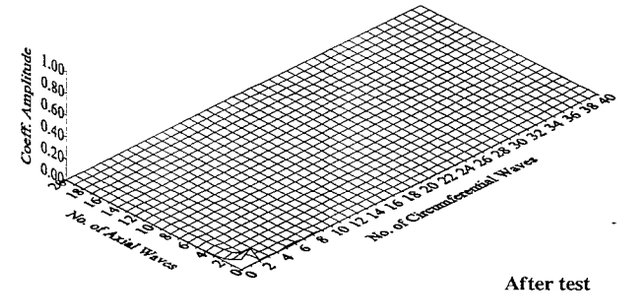

After test

Figure 8 - Two-dimensional Fourier analysis : $[45/-45]_S$ cylinder (normalised to 4.57)

Finite element analysis

The finite element analysis studies numerical models having the same properties as the real specimens, and being able to reproduce the results of the experimental tests, i.e. both the buckling load values and the post-buckling behaviour.
The finite element codes used are ABAQUS and ABAQUS/EXPLICIT[16]. In the case of the implicit code, the buckling is analysed by the eigenvalue and the non-linear Riks methods[17]. The explicit code allows for the investigation of the load-displacement curve, including the post-buckling region, simulating the dynamics of a slow compression test.
ABAQUS (version 5.4) and ABAQUS/EXPLICIT (version 5.5) are implemented on a multiprocessor Convex Exemplar computer.
The cylinders are modelled using 4-nodes bilinear shell elements (ABAQUS element S4R5 and ABAQUS/EXPLICIT element S4R).
The finite element model's length is taken to be 520 *mm*, without the two reinforced tabs. The other geometric dimensions and the material properties are the same as for the real shells. The upper and lower ends of the numerical models are supposed to remain plane and circular, maintaining the initial radius.
After performing mesh convergence studies[15], it was found that 110 elements in the circumferential direction and 26 elements in the axial one is a reasonable choice. Consequently the elements dimensions are 20 x 20 *mm*.

Numerical results

At first, an analysis is performed considering the cylinders without initial imperfections.
The buckling load of axial compression and torsion, obtained by eigenvalue analysis and non-linear Riks method using ABAQUS and by dynamic analysis using ABAQUS/EXPLICIT, are respectively reported in Table 4 and 5.

	Cylinder [0/45/-45/0]	Cylinder $[45/-45]_S$
Analytical solution	240.00	120.58
Eigenvalue analysis ABAQUS	268.43	121.15
Non-linear analysis ABAQUS	266.30	120.23
Dynamic analysis ABAQUS/EXPLICIT	258.92	121.83

Table 4 - Buckling load in axial compression *[kN]*

	Cylinder [0/45/-45/0]	Cylinder $[45/-45]_S$
Eigenvalue analysis ABAQUS	52.44	29.70
Non-linear analysis ABAQUS	51.21	29.18
Dynamic analysis ABAQUS/EXPLICIT	50.92	28.87

Table 5 - Buckling torque in torsion *[kNm]*

Axial compression and torsion, applied individually and in combination, are investigated by eigenvalue analysis using ABAQUS. Both positive and negative torsion is considered. The results for the cylinders with the two different lay-up orientations are presented on Figure 9.
The post-buckling pattern depends on the lay-up orientation and on the value of combined loading, as reported in Figures 10 and 11, where the patterns obtained from the eigenvalue analysis are represented from the case of axial compression (upper) to positive torsion (lower), passing through the cases of combined loading of the interactive curves of Figure 9. The behaviour is different for the two considered cylinders.

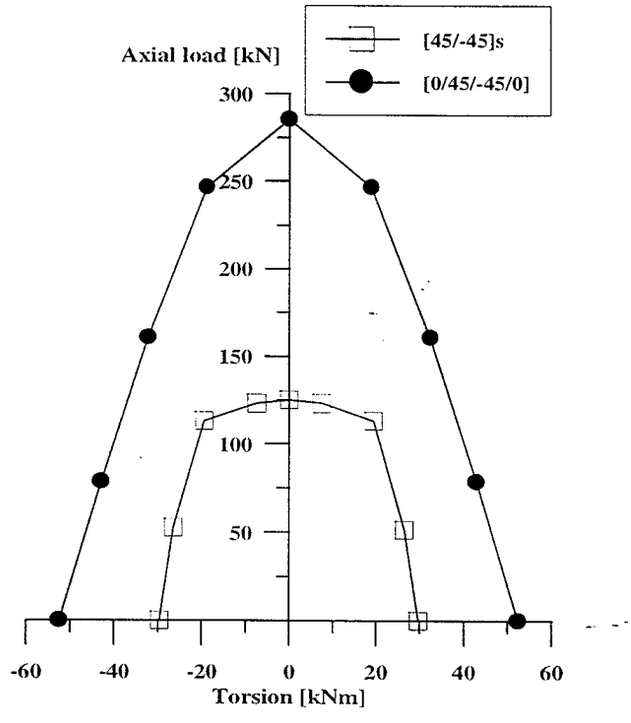

Figure 9 - Eigenvalue analysis for combined loading

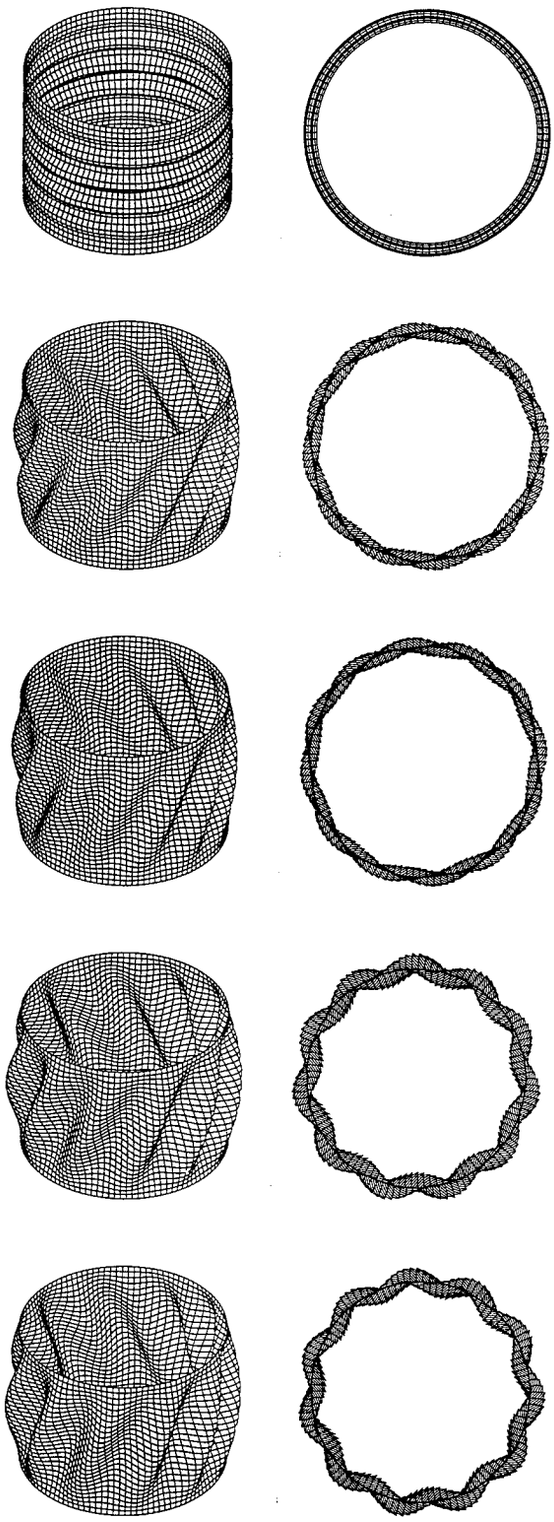

Figure 10-Buckling patterns of [0/45/-45/0] cylinder under axial compression, combined loading and torsion

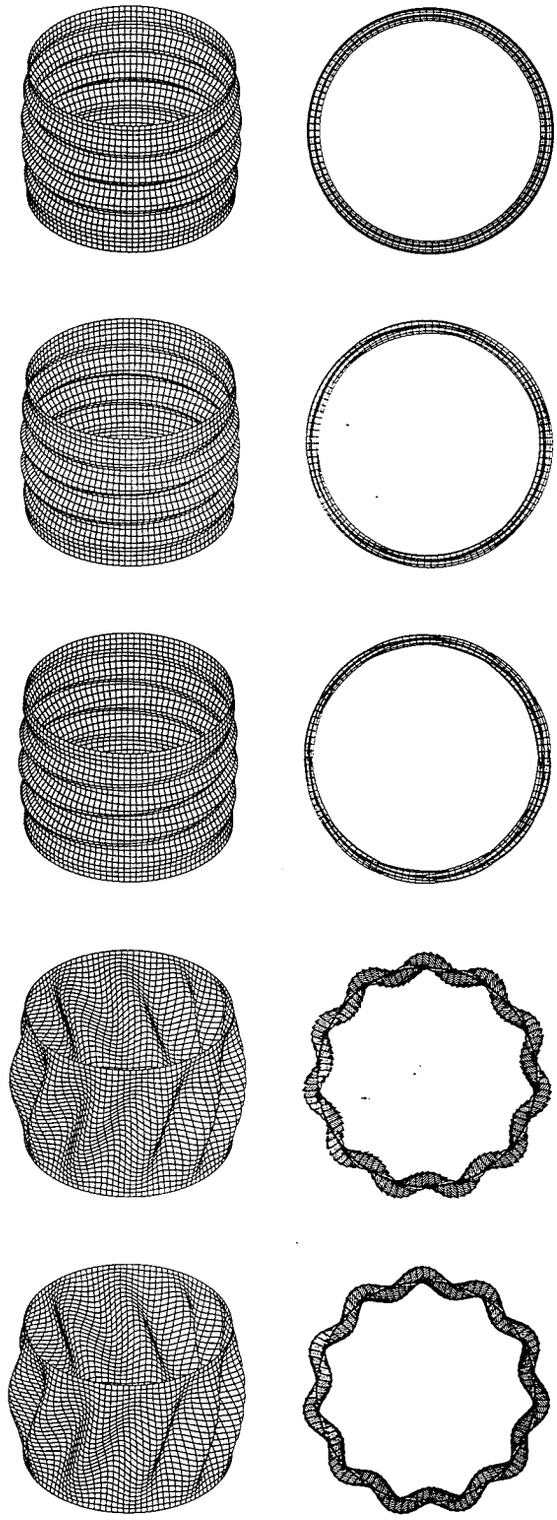

Figure 11 - Buckling patterns of $[45/-45]_S$ cylinder under axial compression, combined loading and torsion

To numerically simulate the experimental buckling tests, the imperfections measured by laser sensors on the internal surface of real specimens before the test are introduced into the finite element models as a perturbation of the perfect cylinder surface.
The experimental measurement of the imperfections is unfortunately limited to the central part of the cylinder surface and the covered area has an axial length of 450 *mm*. In the finite element model, in the zones above and below this central part, the perturbation of the perfect cylinder is assumed to be a linear variation from the imperfections measured at the edge of this central part to zero imperfections, in correspondence to the upper and lower ends of the cylinder.
The results of a numerical analysis, based on an experimental test under axial compression on a cylinder with lay-up orientation [0/45/-45/0], are presented in Figure 12, where the axial reaction force vs. the imposed displacement curve obtained using ABAQUS/EXPLICIT is shown together with the one measured experimentally. The curves indicate qualitatively the same behaviour, but the numerical buckling load is higher than the experimentally measured one, and also the post-buckling capacity is overestimated compared with experiment.
Besides, in the unloading phase, the numerical analysis keeps a residual displacement, but this is probably due to accumulation of numerical errors, because this gap becomes bigger using finer meshes.

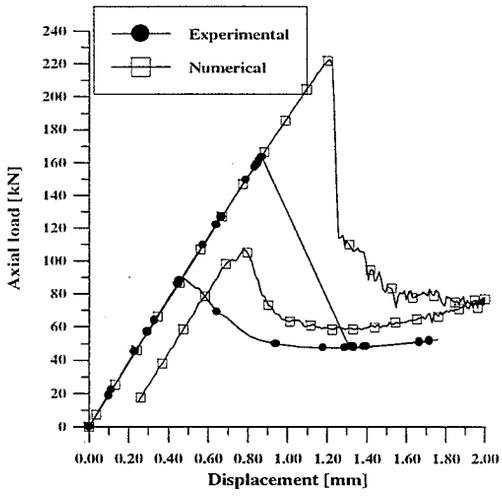

Figure 12 - Experimental - numerical comparison: axial compression buckling test on a [0/45/-45/0] cylinder

An improved value of the buckling load can be obtained using a finer mesh (for example 220x52 elements), but without relevant changes in the post-buckling region.
Better numerical simulations can be obtained considering that, due to the thermal expansion of the metallic mandrel during curing, the carbon fibres tend to concentrate near the inner surface. This effect may reduce the bending stiffness of the shell without affecting the membrane stiffness for the same thickness.
Lower equivalent thicknesses have been considered with the same fibre content (i.e. with the same membrane stiffness), equal to 0.9 and to 0.8 of the nominal thickness, and obtaining results, reported in Figure 13, that are closer to experiment in the post-buckling region.
Of course, this hypothesis have to be confirmed by a microscopic investigation, that will be performed cutting a specimen at the end of all the experimental programme.

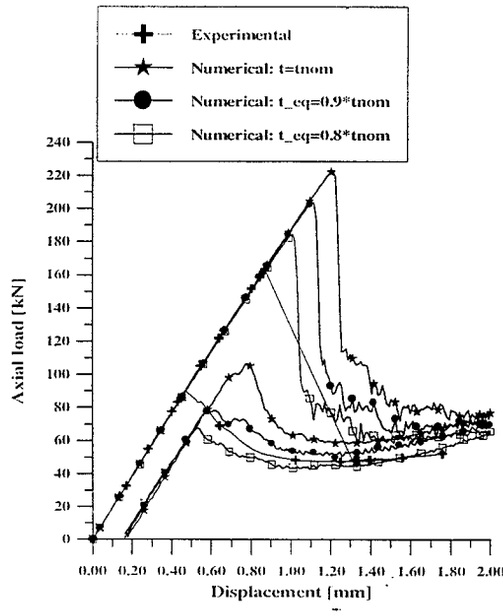

Figure 13 - Numerical analysis considering an equivalent thickness

The numerical analysis performed using ABAQUS/EXPLICIT is able to follow the evolution of the cylinder shape from the buckling to the post-buckling region, as shown in Figure 14 .
It can be seen that the cylinder pass from the undeformed configuration immediately before buckling, to a pattern with a high number of small circumferential waves in correspondence of the buckling load, close to the eigenvector of the linear analysis. At the end, the post-buckling pattern has 9 circumferential waves and 2 axial waves, like that one observed in the experimental test. This is in fair agreement with the high speed film.

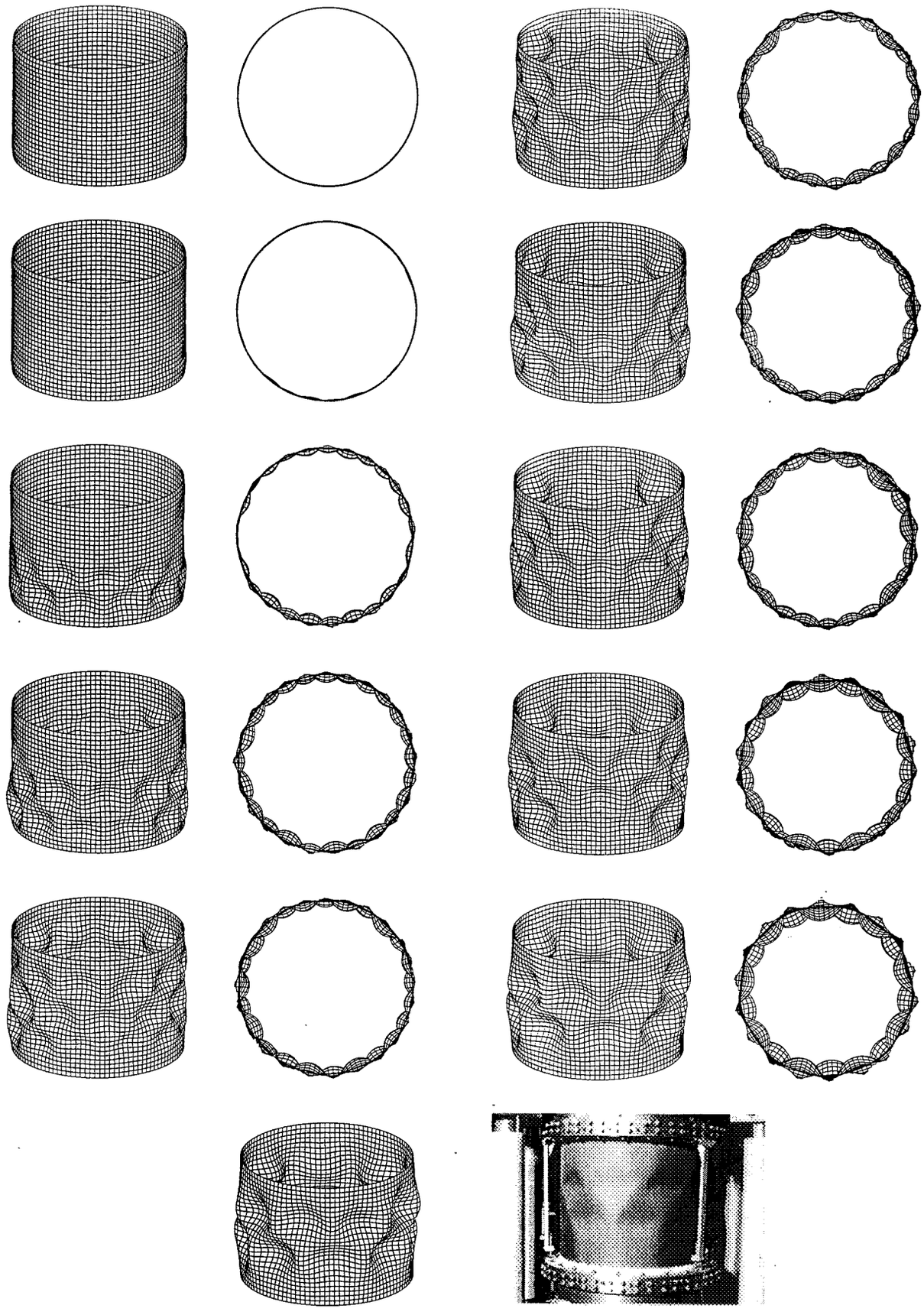

Figure 14 - Evolution of [0/45/-45/0] cylinder pattern in the buckling and post-buckling regions

Analogous numerical analysis, introducing the real imperfections measured by laser sensors on the internal surface of the specimens, are performed under torsion for the two cylinders with the two different lay-up orientations.
Figures 15 and 16 show the torsion vs. the imposed rotation curves obtained for the two cylinders, while Figures 17 and 18 report the corresponding post-buckling pattern.

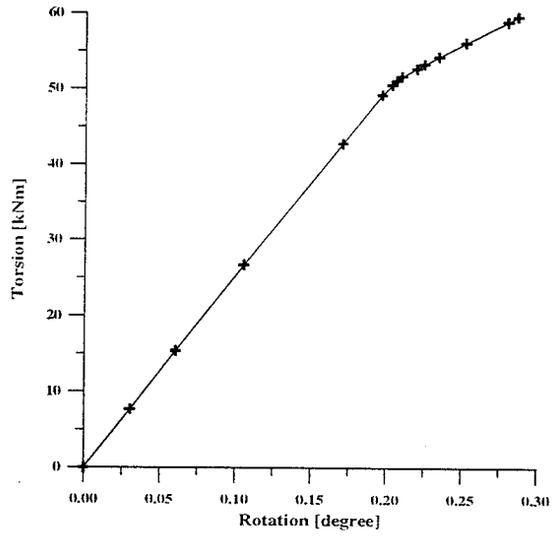

Figure 15 - Numerical torsion buckling test on a [0/45/-45/0] cylinder

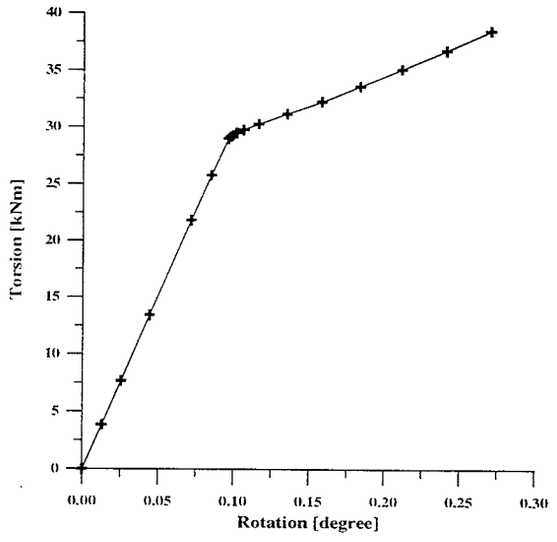

Figure 16 - Numerical torsion buckling test on a $[45/-45]_S$ cylinder

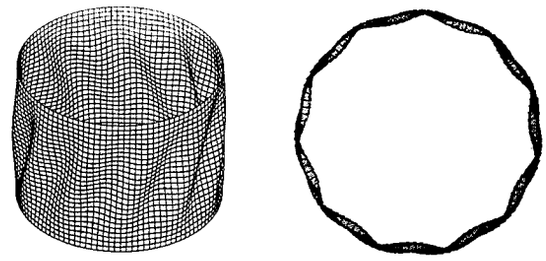

Figure 17 - Torsion post-buckling pattern of a [0/45/-45/0] cylinder

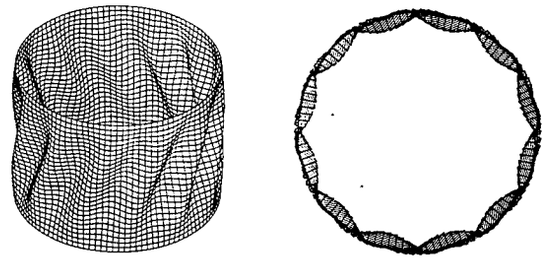

Figure 18 - Torsion post-buckling pattern of a $[45/-45]_S$ cylinder

Conclusions

The results of an experimental and numerical study of the buckling behaviour of carbon-epoxy laminated cylindrical shells have been presented.
The experimental equipment and the methodologies for systematic data acquisition in buckling tests on composite cylindrical shells under axial compression and torsion, applied individually and in combination, have been described.
Typical results of the first tests performed on carbon-epoxy laminated cylinders under axial compression have been presented, in terms of diagrams of compression load vs. axial displacement, post-buckling pattern and two-dimensional Fourier analysis.
A comparison of experimental and analytical buckling loads have been performed and the results show that the ratios between the buckling loads found in tests and the analytical ones are significantly high (around 0.70 for [0/45/-45/0] cylinders and around 0.95 for $[45/-45]_S$ cylinders).
Work is currently under way on performing buckling tests under torsion and under axial compression and torsion applied in combination.
The buckling phenomena has been numerically studied using two finite element codes: ABAQUS and ABAQUS/EXPLICIT.
In the case of the implicit code, the buckling is analysed by the eigenvalue and the non-linear

Riks methods, while the explicit code allows for the investigation of the phenomena, including the post-buckling region, simulating the dynamics of a slow buckling test.
Axial compression and torsion, applied individually and in combination, have been investigated.
The real imperfections measured on the internal surface of the specimens have been introduced in the numerical models and the axial reaction force vs. the imposed displacement curves obtained using ABAQUS/EXPLICIT have been compared to the experimental ones. In particular, the numerical analysis has been able to follow the evolution of the cylinder pattern in the buckling and post-buckling regions, reproducing exactly at the end the experimental post-buckling pattern.
These numerical models, improved by microscopic investigation on fibre distribution and validated by other experimental tests, will allow for a wider study to be performed, investigating the effect of the geometric imperfections and other parameters that may influence the buckling behaviour.

Acknowledgement

The author wishes to express her gratitude to Prof. Vittorio Giavotto, for his helpful suggestions throughout the course of this investigation. She would also like to thank Mr. Francesco Toninelli for his dedicated help. The support provided by the European Commission under a Brite-Euram programme (Project Be-7550: Design and Validation of Imperfection-Tolerant Shell Structures) is gratefully acknowledged

References

1. Kollar L., Dulacska E., *"Buckling of shells for engineers"*, John Wiley & Sons, 1984
2. Simitses G.J., *"Buckling and post-buckling of imperfect cylindrical shells: a review"*, Appl. Mech. Rev., Vol. 39, No. 10, 1986, pp. 1517-1524
3. Jullien J.F. et al., *"Buckling of Shell Structures on Land, in the Sea and in the Air"*, Lyon Symposium, Elsevier Applied Science, 1991
4. *"Buckling of Thin-Walled Circular Cylinders"*, NASA Space Vehicle Design Criteria (Structures), NASA Technical Report SP-8007, 1968
5. *"Buckling of Thin-Walled Doubly Curved Shells"*, NASA Space Vehicle Design Criteria, NASA Technical Report SP-8032, 1969
6. *"European Convention for Constructional Steelwork: Buckling of Steel Shells, European Recommendations"*, Fourth Ed., 1988
7. Elishakoff I. and Arbocz J., *"Reliability of Axially Compressed Cylindrical Shells with General Nonsymmetric Imperfections"*, Journal of Applied Mechanics, Vol. 52, 1985, pp. 122-128
8. Abramovich H., Yaffe R. and Singer J., *"Evaluation of Stiffened Shell Characteristics from Imperfection Measurements"*, Journal of Strain Analysis, Vol. 22, No. 1, 1987, pp.17-23
9. Chryssanthopoulos M., Giavotto V. and Poggi C., *"Characterization of Manufacturing Effects for Buckling-Sensitive Composite Cylinders"*, Composites Manufacturing, Vol. 6, No. 2, 1995, pp. 93-101
10. Simitses G.J., Shaw D. and Sheinman I., *"Stability of Imperfect Laminated Cylinders: a Comparison between Theory and Experiments"*, AIAA Journal, Vol. 23, No. 7, 1985, pp. 1086-1092
11. Abu-Farsakh G, *"Experimental Buckling of GRP Cylindrical Shells"*, Experimental Mechanics, Vol. 27, No. 3, 1987
12. Geier B., Klein H. and Zimmermann R., *"Buckling Tests with Axially Compressed Unstiffened Cylindrical Shells made from CFRP"*, Buckling of Shell Structures on Land, in the Sea and in the Air, edited by J. F. Jullien, Lyon Symposium, Elsevier Applied Science, 1991, pp. 498-507
13. Kweon J.K., Hong C.S. and Lee I.C., *"Post-buckling Compressive Strength of Graphite/Epoxy Laminated Cylindrical Panels Loaded in Compression"*, AIAA Journal, Vol. 33, No. 2, 1995, pp. 217-222
14. Bisagni C., *"Buckling and Post-Buckling Behaviour of Composite Cylindrical Shells"*, XX ICAS Congress, Sorrento (Italy), 1996
15. Bisagni, C., *"Instabilità e Comportamento Post-Critico di Gusci in Materiale Composito"*, Ph.D. Thesis (in Italian), Department of Aerospace Engineering, Politecnico di Milano, 1997
16. *Abaqus, Theory and User's Manual*, Hibbit, Karlsson and Sorensen, Providence, Rhode Island, 1995
17. Riks E., *"An incremental Approach to the Solution of Snapping and Buckling Problems"*, International Journal Solids Structures, Vol. 15, 1979, pp. 529-551